

PAPER • OPEN ACCESS

## Microplastic pollution monitoring with holographic classification and deep learning

To cite this article: Yanmin Zhu *et al* 2021 *J. Phys. Photonics* **3** 024013

View the [article online](#) for updates and enhancements.

You may also like

- [Development of a low-cost method for quantifying microplastics in soils and compost using near-infrared spectroscopy](#)  
L Wander, L Lommel, K Meyer et al.
- [Research Status of Microplastics Pollution in Abiotic Environment in China](#)  
Z H Wang and X J Sun
- [Relative exposure to microplastics and prey for a pelagic forage fish](#)  
J M Chavarry, K L Law, A D Barton et al.



## OPEN ACCESS

## RECEIVED

8 December 2020

## REVISED

16 March 2021

## ACCEPTED FOR PUBLICATION

26 March 2021

## PUBLISHED

16 April 2021

Original Content from this work may be used under the terms of the [Creative Commons Attribution 4.0 licence](#).

Any further distribution of this work must maintain attribution to the author(s) and the title of the work, journal citation and DOI.



## PAPER

## Microplastic pollution monitoring with holographic classification and deep learning

Yanmin Zhu<sup>1</sup> , Chok Hang Yeung<sup>2,3</sup> and Edmund Y Lam<sup>1,\*</sup> <sup>1</sup> Department of Electrical and Electronic Engineering, The University of Hong Kong, Pokfulam, Hong Kong SAR, People's Republic of China<sup>2</sup> Department of Civil Engineering, The University of Hong Kong, Pokfulam, Hong Kong SAR, People's Republic of China<sup>3</sup> Centre for Water Technology and Policy, The University of Hong Kong, Pokfulam, Hong Kong SAR, People's Republic of China

\* Author to whom any correspondence should be addressed.

E-mail: [elam@eee.hku.hk](mailto:elam@eee.hku.hk)**Keywords:** digital holography, deep learning, image classification, microplastic pollutant

## Abstract

The observation and detection of the microplastic pollutants generated by industrial manufacturing require the use of precise optical systems. Digital holography is well suited for this task because of its non-contact and non-invasive detection features and the ability to generate information-rich holograms. However, traditional digital holography usually requires post-processing steps, which is time-consuming and may not achieve the final object detection performance. In this work, we develop a deep learning-based holographic classification method, which computes directly on the raw holographic data to extract quantitative information of the microplastic pollutants so as to classify them according to the extent of the pollution. We further show that our method can generalize to the classification task of other micro-objects through cross-dataset validation. Without bulky optical devices, our system can be further developed into a portable microplastics detection system, with wide applicability in the monitoring of microplastic particle pollution in the ecological environment.

## 1. Introduction

Microplastic particulate pollution generated by industrial manufacturing has become a serious environmental problem [1–3]. These plastic particles with a diameter of less than 5 mm have been detected in different places of the world in recent years, including both terrestrial and marine environment. In some industrial processes such as industrial pharmaceuticals, medical wastes such as disposable syringes and catheters will be generated, which contain polyethylene plastics [4]. Inadequate degradation of such medical waste will also lead to the accumulation of microplastic pollutants. Since the outbreak of COVID-19, a large amount of plastic waste has been generated, which further aggravates the pollution due to microplastic particles. The textile industry is also considered to be a major source of fiber microplastics pollutants, with synthetic fibers in the waste water of textile washing [5]. At the same time, microplastic particles have been reported to be much higher in areas where vehicle manufacturing, large packaging companies and office furniture companies are concentrated, compared with non-industrial areas [6]. Microplastic particles can also come from the degradation of large plastics, waste from landfills or incinerators, and emissions from transportation and industry [7]. The continuous accumulation of microplastic pollutants results in serious environmental problems, such as concentration of microplastics in the ocean [3] and soil [4], the death of marine animals [8], etc.

Normally, microplastics are mixed with other particles in the ecological environment, such as gravel and soil particles, microalgae, bubbles, leaf fragments and large plastic waste [8], obfuscating some of their features. Consequently, it is difficult to accurately detect and show the quantitative information of microplastics without expensive optical instrumentation or complicated image processing technologies. Conventional approaches to detect and count microplastic particles normally consist of the following steps:

(1) micro-object sample collection from the ecological environment; (2) sample preparation and handling by biochemical or physical methods [8, 9]; (3) image capturing with optical systems; (4) image pre-processing, manual image examination and sample classification. The latter two steps in particular require expert knowledge, and are time-consuming in general.

Several research groups have explored the optical detection and identification of microplastic particles. Bianco *et al* used the support vector machine to extract the characteristics of microplastics and classify them [10]. Takahashi *et al* combined integrated holography with Raman spectroscopy to identify the microplastics [11]. Compared with conventional 2D images, holograms recorded by the digital holography system contain abundant phase information of the objects [12, 13] which provide the possibility for further image classification. Moreover, with the advent of deep learning, digital holography can automatically improve [14, 15], analyze [16] and classify images by using data training models [17]. However, most of the current classification and identification methods based on digital holography require relatively complex sample pretreatment, image reconstruction, denoising and other steps [18], which increase the complexity of related work and reduce the efficiency of microplastic particle classification.

In this study, we propose a holographic image classification system, which combines deep learning to automatically detect the microplastic particles and classify the images according to their quantitative information, so as to monitor microplastic particle pollution. We first introduce the detailed structure of holographic-classifier convolutional neural network (HC-CNN) layer by layer. Then, we comprehensively evaluate the performance of the network in the classification of microplastic particles, including its ability to extract the features from holographic images, the accuracy, precision and the efficiency of the classification. We also provide details of the HC-CNN training to avoid network overfitting and keep it stable. The classification performance is compared with other leading methods, and the generalization of HC-CNN is evaluated on other cross-dataset tests.

Our main contributions can be summarized as follows:

- We propose a deep learning-based digital in-line holography classification system for automatic detection and classification of the microplastic pollutants.
- The tasks of automatic classification for microplastic particles are accomplished directly based on the raw holograms without extra image pre-processing steps, such as denoising and reconstruction. The system yields good performance in classification accuracy, time consumption, network robustness and across-model generalization.
- We construct a well-labelled hologram dataset and make it publicly available, which fills the gap of open source and well-labeled hologram data in this field.
- The automatic classification of microplastic particles based on our system provides a powerful tool for environmental protection organizations and institutions to control microplastic particles pollution.

## 2. Related work

There are two main approaches for the classification of microplastic particles. One is manual sample screening combined with biological and chemical detection [8, 9]. The other is automatic detection based on imaging and spectroscopy [10, 11, 19, 20]. Because the former often involves several hours or even days of sample staining, precipitation, filtration and other processes, optical imaging methods, such as Raman spectroscopy [11], Fourier infrared spectroscopy [21], environmental scanning electron microscopy [9], digital holography [12], etc, have become the focus of researchers in recent years because of their ability to achieve non-contact rapid imaging and object classification. Among them, holographic images have abundant phase information and image features that can be extracted, which is beneficial to improve the accuracy of microplastics classification. Based on the advantages of holographic technology, our laboratory has made a lot of research and exploration in image reconstruction [22], autofocusing [23] and resolution improvement [24] in the field of digital holography.

One way to achieve digital hologram classification of microplastic particles is by manual feature extraction and then classification based on machine learning such as support vector machines [10, 25]. On the other hand, our method leverages a deep learning network to provide better feature extraction and higher classification efficiency, paving the way for real-time classification of microplastics particle and microplastic pollution monitoring. Compared with other deep learning detection method such as that proposed by Wu *et al* [26], our method does not require image autofocusing and reconstruction, which simplifies the processing steps and can achieve quick detection.

The work reported here builds upon our previous publications on the detection and classification of microplastic particles [20, 27, 28]. In [20], we focus on the classification task with a small and imbalanced dataset. We develop deep transfer learning to enhance the feature extraction capability of the CompNet,

which is a specially designed network for small dataset classification. Then, in [27], a generative adversarial network is used for an effective holographic image augmentation and dataset expansion. Both methods tackle the situation with a small dataset and insufficient image labeling, which is different from the training and classification of the well-labeled larger dataset in the present work. The data augmentation by transfer learning [20] and generative adversarial network [27] not only cannot guarantee that augmented images contain valid features, but also consume additional computing resources and slow down the classification speed when dealing with well-labeled datasets. The detailed classification performance comparisons will be shown in detail in section 4.

On the other hand, this work can be considered as a further extension of that presented in [28]. The detection and classification of microplastic particles are handled by using a specially designed HC-CNN based on a single raw hologram without image pre-processing steps, such as denoising and reconstruction. In addition, here we introduce the network structure and training process of HC-CNN, which is specially designed for the characteristics of microplastic particle holographic images, and comprehensively evaluate the classification performance of this network on various aspects such as accuracy, precision, and recall rate. This paper provides a detailed explanation for the classification method of microplastic particles based on digital holography.

### 3. Holographic classification method with deep learning

A high-level overview of the holographic classification method is shown in figure 1. Firstly, the raw images are captured by the digital in-line holography system, which is shown in figure 1(a). Secondly, these data are well labelled and built into a dataset. Thirdly, this dataset is feed into the specially designed HC-CNN for the model training. And finally, this model is utilized for the microplastic particles classification and monitoring.

#### 3.1. Lensless digital in-line holography system with a low coherence light source

As shown in figure 1(a), the optical system is a lensless digital in-line holography system with an LED (440 nm wavelength and 24 nm bandwidth), a complementary metal oxide semiconductor (CMOS) camera (Mako-507b,  $2464(H) \times 2056(V)$ ,  $3.45 \mu\text{m}$  pixel size) and a sample slide. LEDs consume less energy and are smaller and lighter than laser light sources. We use LED as the illumination, because it will be more suitable for installation in portable devices. The detailed experimental configurations are as follows: the distance between the LED light source and the imaging surface of the CMOS camera is 18.5 cm, and the sample slide is placed 2.5 cm away from the imaging surface. This experimental setup places the camera on the image plane of the system, thus building a unit amplification optical system. The detectable range of the system is about  $100 \mu\text{m}$  to 5 mm.

Mathematically, the optical wave with the object information has a complex amplitude, denoted by:

$$E_o(x, y) = A_o(x, y) \exp(-j\phi_o(x, y)), \quad (1)$$

where  $A_o$  is the amplitude of the object wave and the  $\phi_o$  is the phase. The reference wave has a similar format as the object wave, which can be written as:

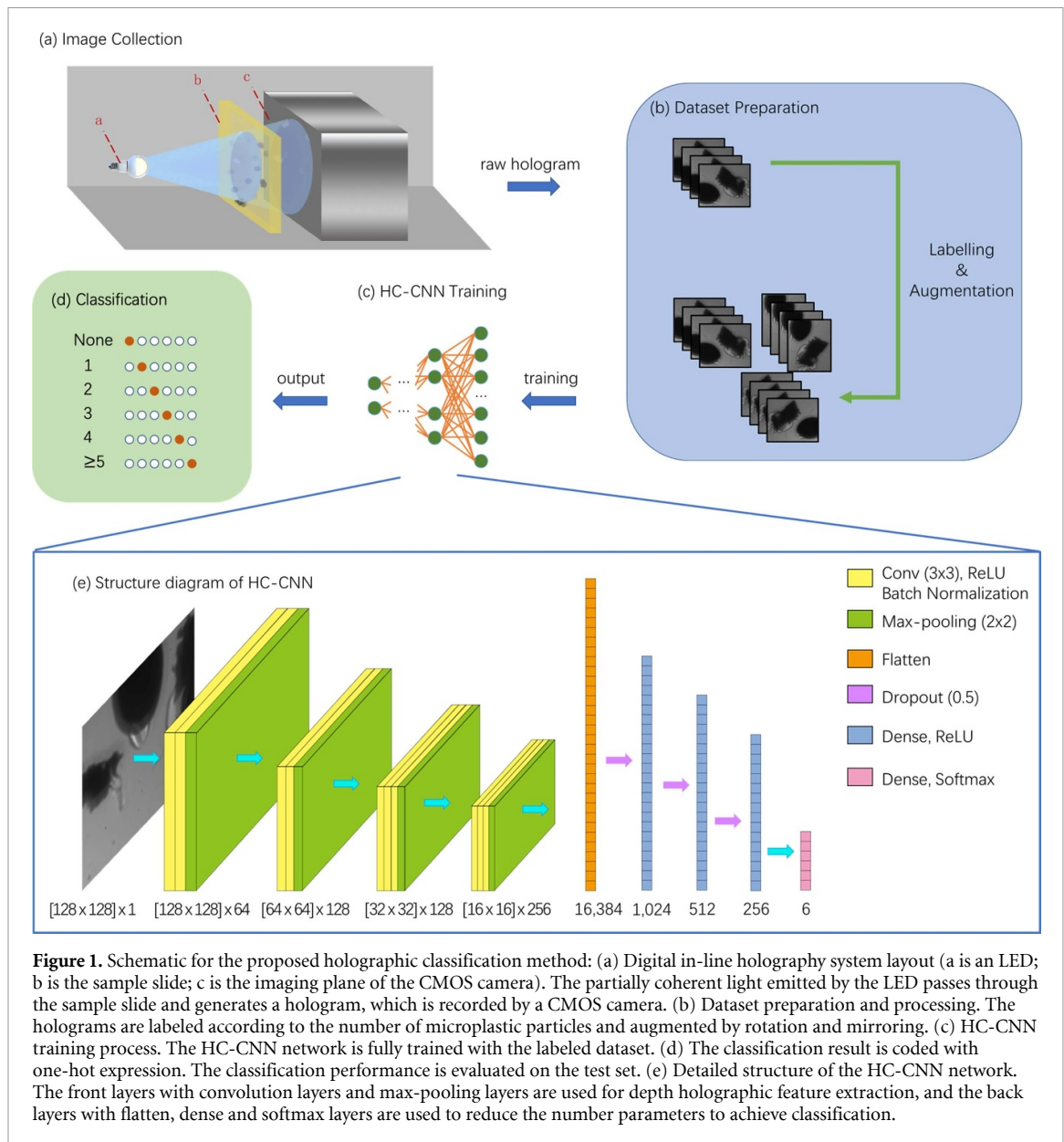
$$E_r(x, y) = A_r(x, y) \exp(-j\phi_r(x, y)), \quad (2)$$

where  $A_r$  and  $\phi_r$  are the amplitude and phase of the reference wave, respectively. During imaging, the reference wave and the object wave travel along the same optical path after being emitted by the LED and form an interference pattern, or a hologram, in the imaging plane. The CMOS camera records the intensity of the hologram, given by [12]:

$$\begin{aligned} I(x, y) &= |E_o(x, y) + E_r(x, y)|^2 \\ &= |E_o(x, y)|^2 + |E_r(x, y)|^2 + E_o(x, y)E_r^*(x, y) + E_o^*(x, y)E_r(x, y), \end{aligned} \quad (3)$$

where  $*$  denotes complex conjugation. It is worth noting that  $|E_o(x, y)|^2$  and  $|E_r(x, y)|^2$  are the zero-order terms, which contribute to the background of the hologram. The interference terms  $E_o(x, y)E_r^*(x, y)$  and  $E_o^*(x, y)E_r(x, y)$  are complex. Therefore, holograms contain more information, which require more complex processing for full feature extraction.

Compared with other traditional optical holography systems [12], such as off-axis digital holography and optical scanning holography, our system does not need bulky optical devices. In addition, the presence of optical devices, such as the microscope objective, beam splitter cube and lenses, may introduce the aberrations [29] including wavefront curvature, spherical aberration, chromatic aberration and astigmatism in mobile use, which will dramatically reduce the image resolution and affect the image quality. In order to



ensure a stable imaging performance, we put the CMOS camera as close to the sample as possible, and remove the microscope objective and external lenses. Furthermore, because the reference light and object light travel along the same optical path, the influence of the external jitter can be counteracted.

### 3.2. Holographic-classifier convolutional neural network

The HC-CNN network is specially designed for the task of microplastic particle classification considering the following characteristics of the dataset:

- Holograms contain richer information than digital images, so it is necessary to make full use of the features by a deeper feature extraction network structure.
- The number of category of the hologram dataset is relatively few. A light network structure and appropriate network parameters are needed to avoid network over-fitting.
- In order to achieve the goal of real-time detection, the convergence time of the network needs to be relatively short.

As shown in figure 1(e), to fully extract the abundant phase information features, we use more convolution layers in the upper part of the network. At the same time, to avoid over-fitting of the network, the Max-pooling layer is appended to the convolution layers. To realize the real-time classification and speed up the training process, batch normalization layer is utilized in the network. In addition, considering the number of classes in the dataset is relatively small, the dense function is used to drop the excess parameters.

**Table 1.** Distribution of the dataset in terms of the number of microplastic particles (MP) in the hologram.

Class	Number of holograms
1 MP	272
2 MP	99
2 MP	104
4 MP	40
$\geq 5$ MP	32
None	49
Total	596

The final possibility of each class is coded with the expression of one-hot  $\mathbb{O}(c)$ , which is defined as:

$$\mathbb{O}(c) = \begin{cases} 1 & \text{if } c \text{ is the predicted class,} \\ 0 & \text{for all other classes,} \end{cases} \quad (4)$$

where integer  $c \in [1, C]$  for a given number of classes  $C$ . The final possibility of each class is calculated by a softmax function.

In addition, we have found that the abundant features contained in the hologram may not be fully extracted. In order to achieve better parameter and feature matching, we consider various loss functions to assist the training of the network on the hologram dataset without increasing the parameters of the network. Inspired by the work of Demirkaya *et al* [30] on the role of loss functions in multiclass classification problems, we introduce over-parameterization into the network training on hologram dataset and use the correct-class quadratic loss  $\mathcal{L}_{CCQL}$  as the loss function, given by:

$$\mathcal{L}_{CCQL} = \frac{1}{2C} \sum_{c=1}^C \left( \|\mathbb{O}(c) - G(c)\|_2^2 + \alpha \|1 - G(c)\|_2^2 \right), \quad (5)$$

where  $G(c)$  is the corresponding label and  $\alpha$  is the weight parameter used to adjust the influence of the correct class on the guidance of the network training process.

### 3.3. Sample selection and preparation

Polyethylene (PE), polystyrene (PS), low-density polyethylene (LDPE) and high-density polyethylene (HDPE) are the main types of microplastic particles in the world [8] and they are chosen as the detection samples in our experiment. Some industrial processes, such as air-blasting system, may produce a large quantity of PS [6]. Besides, polyhydroxyalkanoate (PHA), one of the new thermoplastic pollutants, is also selected as another detection sample of our experiment. The sample size ranges from 90 to 450  $\mu\text{m}$ . In order to simulate the *in situ* microplastic detection environment, the experimental samples are made of standard microplastic particles mixed with gravel, large plastic fragments, soil particles and leaf fragments. The sample making and mixing process is completed by a professional. Detailed information of the standard microplastic particles we used for our experiments are: HDPE (Sigma-Aldrich #427 985); LDPE (Sigma-Aldrich #428 043); PP (Sigma-Aldrich #427 888); PS (Millipore Sigma GF63567030); PHA (Millipore Sigma GF53774545).

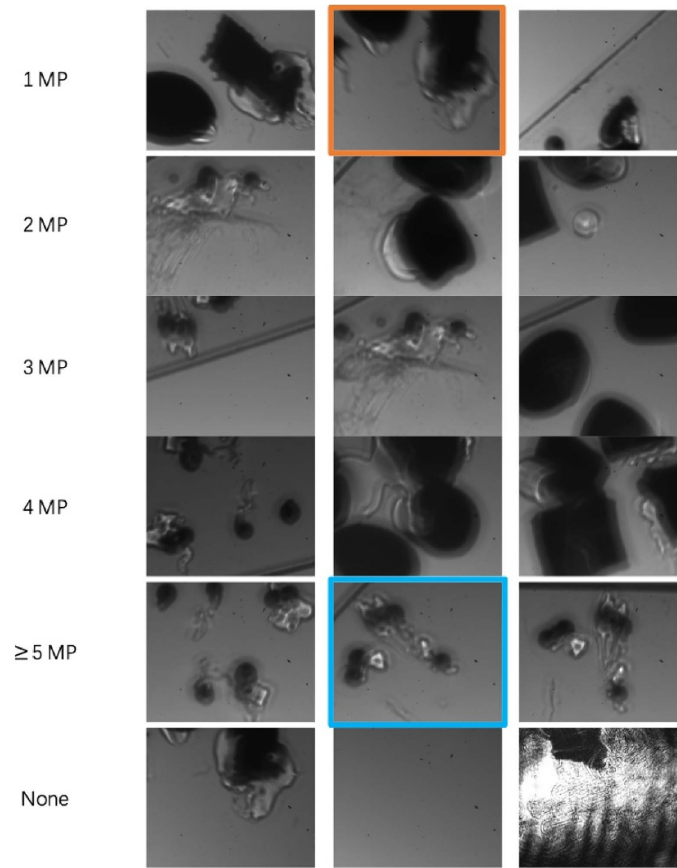
### 3.4. Dataset preparation and labelling

We have built a well-labelled hologram dataset for network training and microplastics classification. We also select several sample holograms for each class from the dataset and show them in figure 2(a). Two zoom-in sample holograms are provided in figures 2(b) and (c) to show the contents of the hologram in more detail. The microplastic is marked as ‘MP’ and the other impurity particles are marked as ‘dust particles’, which have more irregular morphological characteristics compared to the microplastics. The images are labeled according to the preset setting of the corresponding sample at the time of sample making and loading. The class distribution of the dataset is shown in table 1.

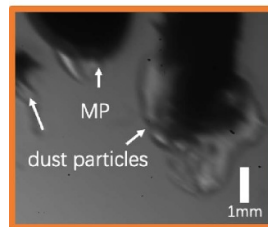
Data augmentation is used to enlarge the dataset for better training of the network. With  $0^\circ$ ,  $90^\circ$ ,  $180^\circ$  and  $270^\circ$  rotations and horizontal mirroring, the final dataset is augmented eight-fold to 4768 images. Then, the dataset is divided into a training set, a validation set, and a test set with a ratio approximately of 8:1:1. To ensure the impartiality and objectivity of the test, the images in the test do not appear in the training and validation.

The network structure is implemented by TensorFlow and the training process is accelerated by NVIDIA TITAN V GPU with a 1455 MHz core frequency. We use the Adam optimizer [31] to update the gradient with a learning rate of 0.0001. In the  $\mathcal{L}_{CCQL}$ , we set  $\alpha = (\sqrt{C-1} - 1)$ , with the logic that the correct-class

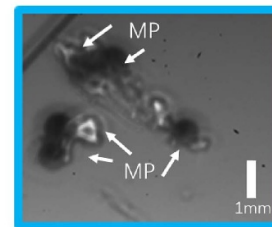




(a)



(b)



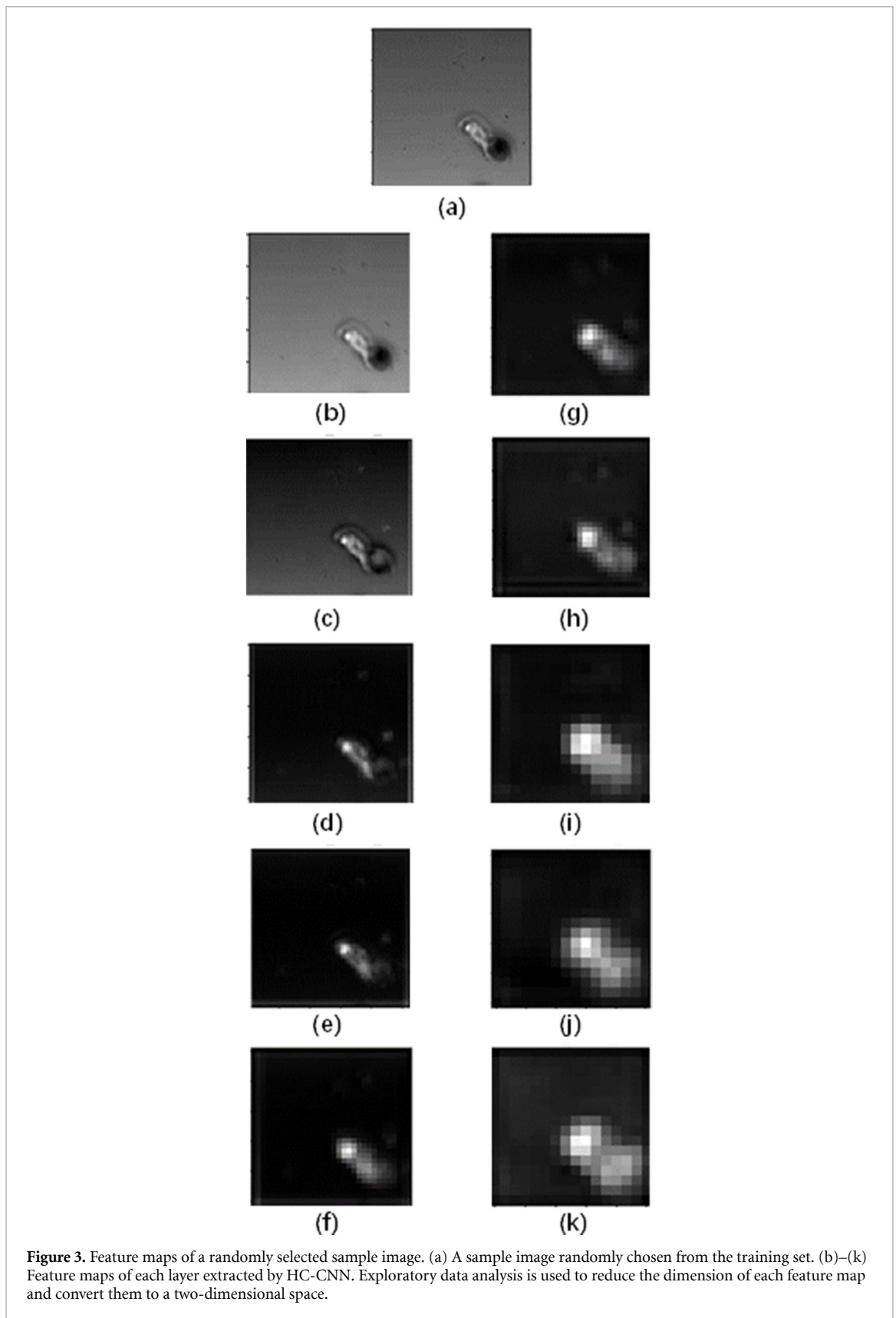
(c)

**Figure 2.** Sample images in the open source dataset. The dataset contains holographic images labeled with the number of microplastics. It can be accessed at [github](https://github.com/yizhu1992/microplastic-hologram-dataset). (a) Labeled raw holograms of different classes. (b) Zoomed in hologram (corresponding to the orange-frame sample image) labeled with microplastics (MP) and dust particles. (c) Zoom-in hologram (corresponding to blue-frame sample image) labeled with MPs.

quadratic loss will automatically assign a weight of  $\alpha + 1$  on the correct class and give a weight of  $C - 1$  to all other classes. The square-root operation is used to reduce the linearity of the function.

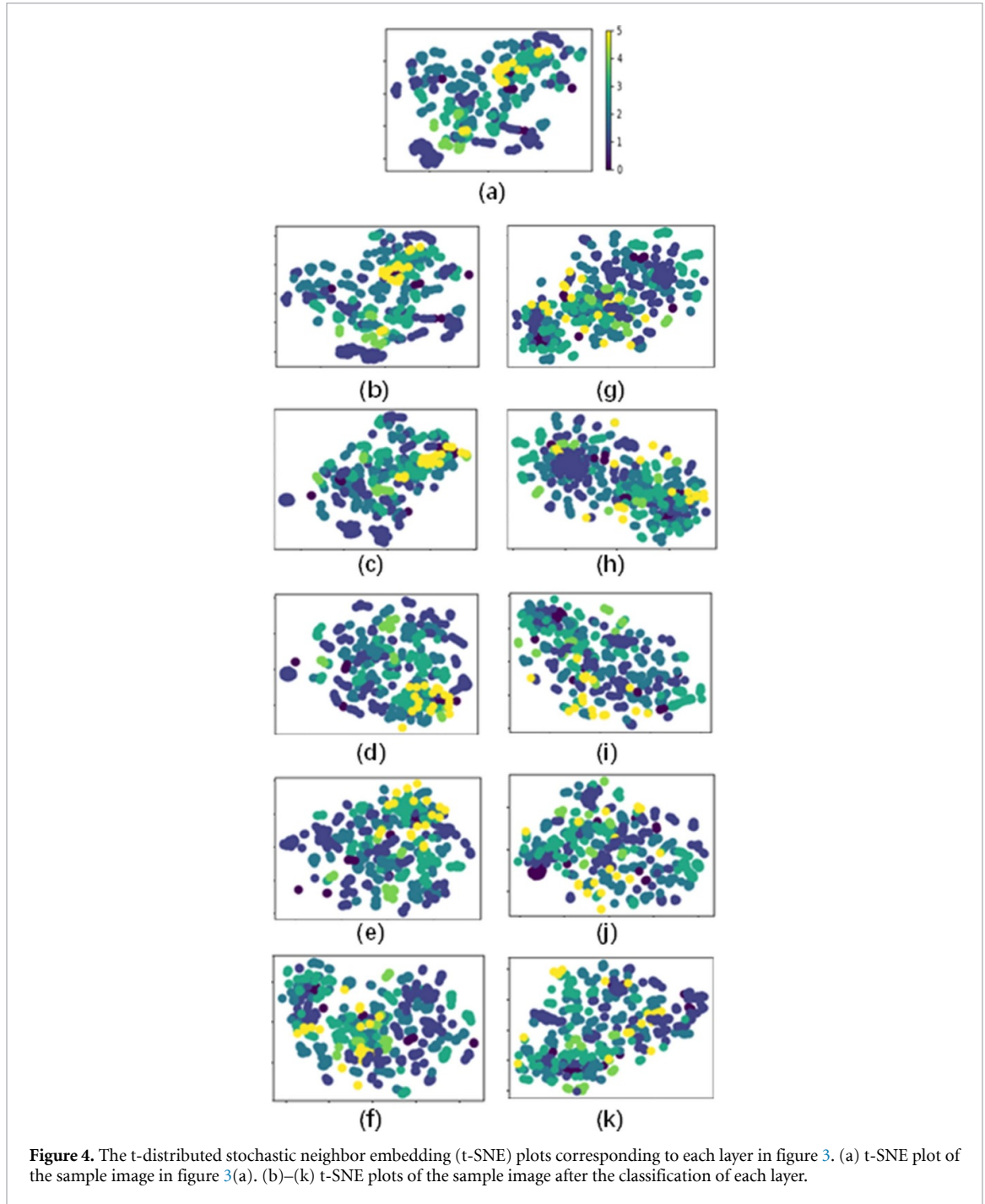
#### 4. Results and discussion

To demonstrate the power of HC-CNN on hologram classification, we show the feature maps of a randomly selected sample image in figure 3, which are extracted by each convolutional layer of the neural network in sequence. In addition, we use EDA (exploratory data analysis) [32] to reduce the dimension of each feature map and convert them to a two-dimensional space, showing with t-distributed stochastic neighbor embedding (t-SNE) plots [33] in figure 4. This is a nonlinear dimensionality reduction tool to show the feature distribution in a 2D or a 3D space. From figures 3(b)–(k), as the number of convolution layer increases, the feature areas in the original hologram become smaller, and the features are effectively extracted. Moreover, figure 4, feature points are more segregated and are easier to classify in (k) than in (a), which is consistent with the results of the corresponding feature maps.



To assess the performance of HC-CNN during the training process more visually, the accuracy and loss of the training set and the validation set with respect to the number of iterations are plotted in figure 5. The validation loss dramatically decreases after about 20 iterations, while the accuracy of the validation set improves quickly. Therefore, the network starts to converge effectively after about 20 iterations. From about 100–130 iterations (region I), both accuracy and loss values of the validation set become more stable. In this

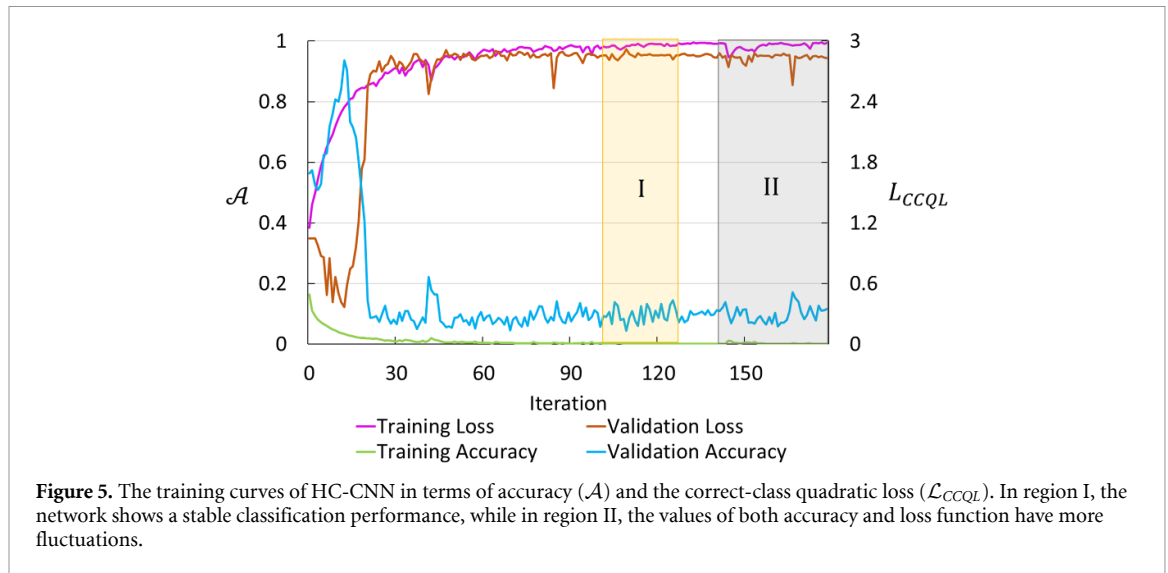




region, the network is well trained and suitable for classification. However, in region II, the data cannot be accurately classified due to the over-fitting of the network, and there are some fluctuations with both accuracy and loss curves. The network may behave worse in this region. On the whole, when the number of iterations of the network is properly controlled to be in region I, the HC-CNN network can show a stable classification performance for microplastic holograms.

In order to compare the performance of HC-CNN network in microplastics classification more objectively, we select other leading methods, namely, multilayer perceptron (MLP) [34], visual geometry group network-16 (VGG-16) [35], CNN, and ResNet [36], and conducted classification tests under the same conditions. For a fair comparison, the parameters of the above-mentioned networks are well adjusted to obtain the best performance. They are evaluated in terms of accuracy ( $\mathcal{A}$ ), precision ( $\mathcal{P}$ ) and recall rate ( $\mathcal{R}$ ), which are calculated by:

$$\mathcal{A} = \frac{X_{TP} + X_{TN}}{H}, \quad (6)$$



$$\mathcal{P} = \frac{X_{TP}}{X_{TP} + X_{FP}}, \quad (7)$$

$$\mathcal{R} = \frac{X_{TP}}{X_{TP} + X_{FN}}, \quad (8)$$

where  $X_{TP}$  represents the HC-CNN output results correctly predicting the well-classified samples,  $X_{TN}$  represents the output correctly predicting the misclassified samples,  $X_{FP}$  represents the output incorrectly predicting the well-classified samples, and  $X_{FN}$  represents the output results incorrectly predicting the misclassified samples.  $H$  is the size of the test set. To evaluate the performance of the classification in some cases where the accuracy and precision cannot be successfully applied, we also use the harmonic mean of  $\mathcal{P}$  and  $\mathcal{R}$ , called F1-score ( $F_1$ ), to measure the accuracy of the classification, which is expressed as:

$$F_1 = \frac{2 \times \mathcal{P} \times \mathcal{R}}{\mathcal{P} + \mathcal{R}}. \quad (9)$$

In addition, the decision time ( $T_D$ ) is measured to assess the computational resources required for classification, which is the sum of the network training time on the training set and the time for the test set classification. The network robustness test is carried out by evaluating 15 repeated independent experiments.

In order to quantitatively compare the performance among different algorithms, we tabulate the values of  $\mathcal{A}$ ,  $\mathcal{P}$ ,  $\mathcal{R}$ ,  $F_1$  and  $T_D$  in table 2. The results of each method are the mean values of fifteen independent experiments. They indicate that HC-CNN network has the highest accuracy, precision, recall rate and F1-score and it also has the smallest variance, demonstrating good robustness of our approach. In spite of the ResNet network showing a close performance with HC-CNN, it takes three times longer than that of the HC-CNN network. HC-CNN network contains more lightweight feature extraction structure, which effectively reduces the time needed for feature extraction and saves computing resources. In addition, though MLP network costs less time than HC-CNN, its accuracy is significantly lower for there is no convolutional layer to accurately extract the features from holograms. We also compare the performance of the methods proposed in our two previous studies [27] and [20] in table 2. Although they have comparable performance as HC-CNN, the decision time ( $T_D$ ) required is far beyond that of the HC-CNN model due to the additional data augmentation. We therefore can conclude that, compared to other tested networks, HC-CNN is an accurate and fast network for microplastics classification, which increases the possibility of further being implemented on a portable device and used for real-time microplastic pollution monitoring.

In order to further analyze the performance of the multi-class classifier quantitatively, we calculate the normalized confusion matrix of the HC-CNN network. As shown in figure 6, with the unbalanced dataset (shown in table 1), the network has good classification performance on the class of 1, 2, 3, 4 and  $\geq 5$  MP, while having only a 17% error rate in the class of 0 MP. This shows that our network is less susceptible to the small and unbalance-distributed dataset.

To evaluate the generalization ability of HC-CNN, we perform the cross dataset validations on an open source hologram data (Wave Glider [37]). It includes 9140 raw holographic images of hemiaulus cells

**Table 2.** Classification performances of MLP [34], VGG-16 [35], CNN, CompNet [20], ResNet [36], Zhu *et al* [27] and HC-CNN.  $\mathcal{A}$ ,  $\mathcal{P}$ ,  $\mathcal{R}$  and  $F_1$  are defined in equations (6)–(9).  $T_D$  is measured in hour.

Methods	$\mathcal{A}$	$\mathcal{P}$	$\mathcal{R}$	$F_1$	$T_D$
MLP [34]	0.6974	0.5376	0.6370	0.6198	<b>0.2500</b>
VGG-16 [35]	0.8524	0.7890	0.7873	0.7737	1.0833
CNN	0.9403	0.9349	0.8897	0.9014	0.6000
CompNet [20]	0.9421	0.9433	0.8901	0.9133	1.2125
ResNet [36]	0.9459	0.9518	0.8863	0.9049	1.0183
Zhu <i>et al</i> [27]	0.9695	0.9755	0.9545	0.9499	1.2325
HC-CNN	<b>0.9701</b>	<b>0.9761</b>	<b>0.9595</b>	<b>0.9520</b>	0.3833

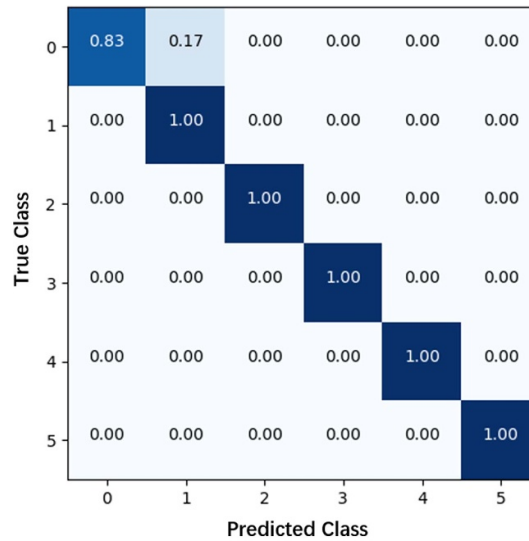


**Figure 6.** The multi-class classification performance is evaluated quantitatively on the normalized confusion matrix of HC-CNN.

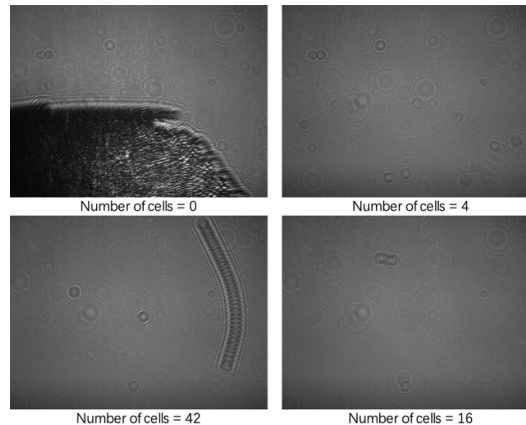


**Figure 7.** Sample images of the open source hologram dataset Wave Glider [37]. The generalization ability of HC-CNN is evaluated with the cross-dataset validation experiment on Wave Glider.

labelled with cell counts and recorded by LISST-Holo Submersible Digital Holographic Camera in 2015. The sample images of Wave Glider are shown in figure 7.

For a fair comparison, we resize the images from Wave Glider to  $128 \times 128$  pixels, which is the same as our own dataset, and re-train all the networks separately. All the training parameters, such as the learning rate, are the same as the training of our own dataset before. The classification accuracies of different networks on Wave Glider are showed in table 3. Compared with other leading methods, HC-CNN also shows higher accuracy on this dataset, which verifies the effectiveness and generalization of HC-CNN on micro-object classifications.

**Table 3.** Cross dataset validation of MLP [34], VGG-16 [35], CNN, CompNet [20], ResNet [36], method proposed in [27] and HC-CNN on Wave Glider [37].

Methods	$\mathcal{A}$	$\mathcal{P}$	$\mathcal{R}$	$F_1$
MLP [34]	0.7674	0.7322	0.7178	0.7022
VGG-16 [35]	0.8399	0.8124	0.7923	0.7856
CNN	0.8901	0.8844	0.8395	0.8462
CompNet [20]	0.9421	0.9321	0.9059	0.9124
ResNet [36]	0.9019	0.8977	0.8759	0.9033
Zhu <i>et al</i> [27]	0.9133	0.9035	0.8876	0.8793
HC-CNN	<b>0.9235</b>	<b>0.9211</b>	<b>0.9135</b>	<b>0.9125</b>

## 5. Conclusion

In this work, we propose a deep learning-enabled lensless digital in-line holography system to automatically detect and classify the microplastic particles directly based on the raw holograms. The performance of this system is experimentally evaluated by training the HC-CNN both on our own hologram dataset and an open source dataset. The experimental results show that our method has good performance in terms of the classification accuracy, network robustness, time efficiency and the generalization ability to other micro-objects.

Future work can be carried out to classify and identify the types of microplastics, since the current classification is only based on their number. In order to better simulate the real environment of underwater microplastic particles, the types of particles in the samples can be more diverse, such as including microalgae and bubbles.

Due to the low complexity of the devices used in this experiment, it can be further developed to be a portable real-time microplastic particle detection device in future experiments. Environmental researchers can use it to monitor microplastic pollutants generated during industrial manufacturing. In addition to microplastic pollutants, our proposed method can also be used for the classification of other micro-objects, such as the particulate pollution (PM<sub>2.5</sub>) monitoring or micro-defects detection on an integrated circuit. Additionally, our work is a good example that combines the typical optical system with artificial intelligence technologies to improve the imaging performance, which offers an attractive direction for the development of other optical systems, such as light field microscopy [38] and hyperspectral imaging [39].

## Data availability statement


The data that support the findings of this study are openly available at the following URL/DOI: [https://github.com/ymzhu19eee/dataset\\_microplastics](https://github.com/ymzhu19eee/dataset_microplastics).

## Acknowledgment

The work is supported in part by the Research Grants Council of Hong Kong (GRF 17201818, 17200019), the University of Hong Kong Interdisciplinary KE Project Fund (KE-ID-2018/19-17) and Environment and Conservation Fund (ECF Project 109/2019).

## ORCID iDs

Yanmin Zhu  <https://orcid.org/0000-0002-3968-5372>

Chok Hang Yeung  <https://orcid.org/0000-0003-2448-5965>

Edmund Y Lam  <https://orcid.org/0000-0001-6268-950X>

## References

- [1] Thompson R C *et al* 2004 Lost at sea: where is all the plastic? *Science* **304** 838
- [2] Rillig M C and Lehmann A 2020 Microplastic in terrestrial ecosystems *Science* **368** 1430–1
- [3] do Sul J A I and Costa M F 2014 The present and future of microplastic pollution in the marine environment *Environ. Pollut.* **185** 352–64
- [4] Hale R C, Seeley M E, La Guardia M J, Mai L and Zeng E Y 2020 A global perspective on microplastics *J. Geophys. Res.: Oceans* **125** e2018JC014719
- [5] Deng H, Wei R, Luo W, Hu L, Li B, Di Y and Shi H 2020 Microplastic pollution in water and sediment in a textile industrial area *Environ. Pollut.* **258** 113658
- [6] Mani T, Hauk A, Walter U and Burkhardt-Holm P 2015 Microplastics profile along the Rhine River *Sci. Rep.* **5** 1–7

- [7] Chen G, Feng Q and Wang J 2020 Mini-review of microplastics in the atmosphere and their risks to humans *Sci. Total Environ.* **703** 135504
- [8] Silva A B, Bastos A S, Justino C I, da Costa J P, Duarte A C and Rocha-Santos T A 2018 Microplastics in the environment: challenges in analytical chemistry—a review *Anal. Chim. Acta* **1017** 1–19
- [9] Zarfl C 2019 Promising techniques and open challenges for microplastic identification and quantification in environmental matrices *Anal. Bioanal. Chem.* **411** 3743–56
- [10] Bianco V, Memmolo P, Carcagnì P, Merola F, Paturzo M, Distante C and Ferraro P 2019 Microplastic identification via holographic imaging and machine learning *Adv. Intell. Syst.* **2** 1900153
- [11] Takahashi T, Liu Z, Thevar T, Burns N, Mahajan S, Lindsay D, Watson J and Thornton B 2020 Identification of microplastics in a large water volume by integrated holography and Raman spectroscopy *Appl. Opt.* **59** 5073–8
- [12] Goodman J W 2017 *Introduction to Fourier Optics* 4th edn (San Francisco, CA: Freeman)
- [13] Ren Z, Zeng T and Lam E Y 2019 Digital holographic imaging via deep learning OSA *Topical Meeting in Computational Optical Sensing and Imaging (Munich, Germany, 24–27 June 2019)* p CTu3A.4
- [14] Ren Z, Xu Z and Lam E Y 2018 Autofocusing in digital holography using deep learning *Proc. SPIE* **10499** 104991V
- [15] Ren Z, Zhao J and Lam E Y 2019 Automatic compensation of phase aberrations in digital holographic microscopy based on sparse optimization *APL Photonics* **4** 110808
- [16] Tsang P W M and Lam H 2019 Holographic vision system based on non-diffractive optical scanning holography and deep learning *Proc. SPIE* **11188** 111880F
- [17] Rivenson Y, Wu Y and Ozcan A 2019 Deep learning in holography and coherent imaging *Light: Sci. Appl.* **8** 1–8
- [18] Lam E Y 2018 Computational imaging and reconstruction in digital holographic microscopy *Proc. SPIE* **10711** 1071104
- [19] Zhu Y, Yeung C H and Lam E Y 2020 Automatic detection of microplastics by deep learning enabled digital holography OSA *Topical Meeting in Digital Holography and Three-Dimensional Imaging (Washington, DC USA, 22–26 June 2020)* p HTu5B.1
- [20] Zhu Y, Yeung C H and Lam E Y 2021 Digital holographic imaging and classification of microplastics using deep transfer learning *Appl. Opt.* **60** A38–47
- [21] Kedzierski M, Falcou-Préfol M, Kerros M E, Henry M, Pedrotti M L and Bruzard S 2019 A machine learning algorithm for high throughput identification of FTIR spectra: application on microplastics collected in the Mediterranean Sea *Chemosphere* **234** 242–51
- [22] Ren Z, Xu Z and Lam E Y 2019 End-to-end deep learning framework for digital holographic reconstruction *Adv. Photonics* **1** 016004
- [23] Ren Z, Xu Z and Lam E Y 2018 Learning-based nonparametric autofocusing for digital holography *Optica* **5** 337–44
- [24] Ren Z, So H K and Lam E Y 2019 Fringe pattern improvement and super-resolution using deep learning in digital holography *IEEE Trans. Ind. Inf.* **15** 110808
- [25] Chaczko Z, Wajs-Chaczko P, Tien D and Haidar Y 2019 Detection of microplastics using machine learning *Int. Conf. Machine Learning and Cybernetics (Kobe, Japan, 7–10 July 2019)* (IEEE) pp 1–8
- [26] Wu Y et al 2018 Label-free bioaerosol sensing using mobile microscopy and deep learning *ACS Photonics* **5** 4617–27
- [27] Zhu Y, Yeung C H and Lam E Y 2020 Digital holography with deep learning and generative adversarial networks for automatic microplastics classification *Proc. SPIE* **11551** 115510A
- [28] Zhu Y, Yeung C H and Lam E Y 2020 Holographic classifier: deep learning in digital holography for automatic micro-objects classification *IEEE Int. Conf. Industrial Informatics* pp 516–20
- [29] Colomb T et al 2006 Numerical parametric lens for shifting, magnification and complete aberration compensation in digital holographic microscopy *J. Opt. Soc. Am. A* **23** 3177–90
- [30] Demirkaya A, Chen J and Oymak S 2020 Exploring the role of loss functions in multiclass classification 2020 54th Conf. Information Sciences and Systems (CISS) (Princeton, NJ, USA, 18–20 March 2020) (IEEE) pp 1–5
- [31] Goodfellow I, Bengio Y and Courville A 2016 *Deep Learning* (Cambridge, MA: MIT Press)
- [32] Tukey J W 1977 *Exploratory Data Analysis* 1st Boston, MA: Addison-Wesley
- [33] Maaten L V D and Hinton G 2008 Visualizing data using t-SNE *J. Mach. Learn. Res.* **9** 2579–605
- [34] Bourlard H and Kamp Y 1988 Auto-association by multilayer perceptrons and singular value decomposition *Biol. Cybern.* **59** 291–4
- [35] Simonyan K and Zisserman A 2014 Very deep convolutional networks for large-scale image recognition (arXiv:1409.1556)
- [36] Szegedy C, Ioffe S, Vanhoucke V and Alemi A A 2017 Inception-v4, inception-resnet and the impact of residual connections on learning *Proc. AAAI Conf. on Artificial Intelligence February 2017* vol 31 p 1
- [37] Cara W and Tracy A V 2018 Holographic images from LISST-Holo system while deployed on the AUV Honey Badger (Wave Glider) during a deployment in the North Pacific Gyre in 2015 (MAGI project) Biological and Chemical Data Management Office (available at: [www.bco-dmo.org/dataset-deployment/718410/data](http://www.bco-dmo.org/dataset-deployment/718410/data))
- [38] Meng N, Zeng T and Lam E Y 2019 Spatial and angular reconstruction of light field based on deep generative networks *IEEE Int. Conf. Image Processing (Taipei, Taiwan, 22–25 September 2019)* pp 4659–63
- [39] Chang C-I 2003 *Hyperspectral Imaging: Techniques for Spectral Detection and Classification* vol 1 (New York: Springer) (<https://doi.org/10.1007/978-1-4419-9170-6>)